2D Serre-Green-Naghdi Equations over Topography: Elliptic Operator Inversion Method

Sergey Gavrilyuk[1] and Keh-Ming Shyue[2]

Abstract: Multidimensional Serre–Green–Naghdi equations are numerically solved by using a natural hyperbolic-elliptic splitting. The hyperbolic step is solved by semidiscret finite volume methods. The elliptic step is related to recovering nonhydrostatic pressure. One-dimensional (1D) and two-dimensional (2D) test problems (i.e., 1D solitary wave propagation, 2D dam-break problem, solitary wave overstep and overhump) are considered. **DOI: 10.1061/JHEND8.HYENG-13703.**

Introduction

We describe a simple hyperbolic-elliptic splitting approach for the efficient numerical resolution of the Serre–Green–Naghdi (SGN) equations for shallow water flows in more than one space dimension. The SGN equations can be derived by depth averaging of the free surface Euler equations (Serre 1953; Su and Gardner 1969; Green et al. 1974; Green and Naghdi 1976; Bazdenkov et al. 1987; Camassa et al. 1996; Liapidevskii and Gavrilova 2008; Li et al. 2019; Castro-Orgaz and Hager 2017) and via Hamilton's principle of stationary action (Miles and Salmon 1985; Salmon 1998; Barros et al. 2007; Busto et al. 2021). The SGN equations can also be seen as a special case in a hierarchy of vertically averaged high-order models (Castro-Orgaz et al. 2023). The SGN model augmented by the wave-breaking dissipation terms is proposed in (Cienfuegos 2023).

In dimensional form, the SGN equations are

$$h_t + \mathrm{div}(h\bar{\mathbf{v}}) = 0 \tag{1a}$$

$$(h\bar{\mathbf{v}})_t + \mathrm{div}\left(h\bar{\mathbf{v}}\otimes\bar{\mathbf{v}} + \left(\frac{gh^2}{2} + \frac{h^2}{3}\left(\ddot{h} + \frac{3}{2}\ddot{b}\right)\right)\mathbf{I}\right) = -p|_{z=b}\nabla b \tag{1b}$$

$$(h\mathcal{E})_t + \mathrm{div}\left(h\bar{\mathbf{v}}\mathcal{E} + \left(\frac{gh^2}{2} + \frac{h^2}{3}\left(\ddot{h} + \frac{3}{2}\ddot{b}\right)\right)\bar{\mathbf{v}}\right) = p|_{z=b} b_t \tag{1c}$$

with

$$p|_{z=b} = gh + h\left(\ddot{b} + \frac{1}{2}\ddot{h}\right) \tag{1d}$$

$$\mathcal{E} = \frac{|\bar{\mathbf{v}}|^2}{2} + g\left(\frac{h}{2} + b\right) + \frac{1}{6}\left(\dot{h} + \frac{3}{2}\dot{b}\right)^2 + \frac{1}{8}\dot{b}^2 \tag{1e}$$

where h = the water depth; $\bar{\mathbf{v}}$ = the depth averaged velocity; g = the gravity acceleration; b = the bottom topography; and $z = h + b$ = the free surface (see Fig. 1). The "dot" means the material derivative along the averaged velocity $\bar{\mathbf{v}}$: $\dot{f} = (\partial f/\partial t) + \bar{\mathbf{v}}\cdot\nabla f$ for any scalar function $f(t, \mathbf{x})$; two "dots" mean the corresponding second material derivative (see Appendix for details).

The difficulty in solving the momentum equation in the form in Eq. (1b) is that its flux depends on the time derivatives of $\bar{\mathbf{v}}$. To overcome this difficulty, one introduces the variable $\mathbf{K}$ defined as

$$\mathbf{K} = \frac{1}{h}\frac{\partial L}{\partial \bar{\mathbf{v}}} = \bar{\mathbf{v}} + \frac{1}{3}\left(\dot{h} + \frac{3}{2}\dot{b}\right)\nabla h + \left(\frac{1}{2}\dot{h} + \dot{b}\right)\nabla b \tag{2}$$

where the Lagrangian $L(\bar{\mathbf{v}}, h, \dot{h}, b, \dot{b})$ is defined by Eq. (60). The quantity $\mathbf{K}$ is more important than $\bar{\mathbf{v}}$. In particular, it verifies the Helmholtz equation, and its circulation along closed material lines is conserved in time (generalized Kelvin's theorem) (Gavrilyuk and Teshukov 2001). In addition, by introducing the generalized flow potential ϕ by $\mathbf{K} = \nabla\phi$, one can reduce the study of SGN equations to the study of two scalar equations for the fluid depth h and the flow potential ϕ (Gavrilyuk and Teshukov 2001). The choice of $\mathbf{K}$, which is defined up to the gradient of an arbitrary function, is not unique, however. For example, using the mass conservation law in Eq. (1a) one can rewrite Eq. (2) in the form

$$\mathbf{K} = \bar{\mathbf{v}} - \frac{1}{3h}\nabla(h^3\mathrm{div}(\bar{\mathbf{v}})) + \frac{1}{3}\nabla(h^2\mathrm{div}(\bar{\mathbf{v}})) + \frac{1}{2h}\nabla(h^2\dot{b}) - \frac{1}{2}\nabla(h\dot{b}) + \left(\frac{1}{2}\dot{h} + \dot{b}\right)\nabla b \tag{3}$$

Hence, up to the gradient terms, one can replace Eq. (3) by

$$\mathbf{K} = \bar{\mathbf{v}} - \frac{1}{3h}\nabla(h^3\mathrm{div}(\bar{\mathbf{v}})) + \frac{1}{2h}\nabla(h^2\dot{b}) + \left(\frac{1}{2}\dot{h} + \dot{b}\right)\nabla b \tag{4}$$

In particular, in the case of a flat bottom, the sum of the two first terms in Eq. (4), $\bar{\mathbf{v}} - (1/3h)\nabla(h^3\mathrm{div}(\bar{\mathbf{v}}))$ is the tangent velocity of the fluid at the free surface (Gavrilyuk et al. 2014).

We illustrate the advantages of using $(h, \mathbf{K})$ variables in the 1D formulation. By using Eq. (4), the momentum [Eq. (1b)] can be written in conservative form even in the case of time dependent bottom $b(t, x)$ as

$$K_t + \left(KU + g(b+h) - \frac{1}{2}(\dot{b} + \dot{h})^2 - \frac{1}{2}U^2\right)_x = 0 \tag{5}$$

where U is the horizontal depth averaged velocity [$\bar{\mathbf{v}} = (U, 0)^T$], and

[1]Professor, Dept. of Mechanics, Aix Marseille Univ., Centre National de Recherche (CNRS), Institut Universitaire des Systèmes Thermiques Industriels (IUSTI), Unité Mixte de Recherche (UMR) 7343, Marseille 13004, France (corresponding author). ORCID: https://orcid.org/0000-0003-4605-8104. Email: sergey.gavrilyuk@univ-amu.fr

[2]Professor, Institute of Applied Mathematical Sciences, National Taiwan Univ., Taipei 106, Taiwan. ORCID: https://orcid.org/0000-0002-9846-5054. Email: shyue@ntu.edu.tw

Note. This manuscript was submitted on March 17, 2023; approved on July 26, 2023; published online on October 18, 2023. Discussion period open until March 18, 2024; separate discussions must be submitted for individual papers. This paper is part of the ***Journal of Hydraulic Engineering***, © ASCE, ISSN 0733-9429.

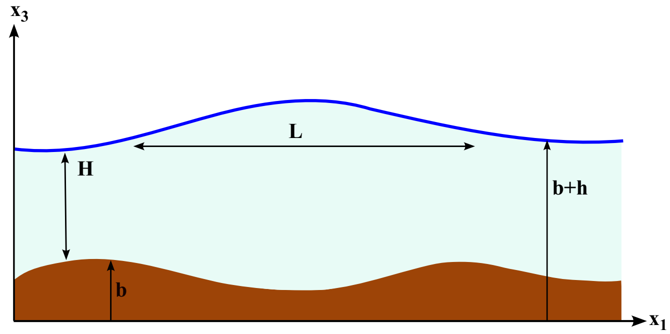

Fig. 1. Sketch of the flow over topography.

$$K = U - \frac{1}{3h}(h^3 U_x)_x + \frac{1}{2h}(h^2 \dot{b})_x + \left(\frac{1}{2}\dot{h} + \dot{b}\right) b_x \tag{6}$$

Replacing $\dot{h} = -U h_x$ in Eq. (5), one obtains the flux depending on U and its space derivatives, space derivatives of h, and time and space derivatives of $b(t,x)$. Once K and h are updated at a new time instant by any solver, the velocity U at this time instant is obtained from Eq. (6) by inverting the corresponding 1D elliptic operator (Le Métayer et al. 2010; Cantero-Chinchilla et al. 2016; Castro-Orgaz et al. 2022).

To find $\bar{\mathbf{v}}$ from Eq. (4) in the 2D case, we have to invert two elliptic operators (one for each component of $\bar{\mathbf{v}}$) at each time, which is computationally the most "expensive" step (Le Métayer et al. 2010; Li et al. 2014, 2019; Marche 2020).

To avoid the elliptic step in solving the SGN equations, another idea was proposed based on their hyperbolic approximation (Favrie and Gavrilyuk 2017; Busto et al. 2021; Tkachenko et al. 2023). Such an approximation is related to a modification of the "master" Lagrangian in Eq. (60): a new "extended" Lagrangian is introduced whose Euler–Lagrange equations approximate the SGN equations. Thus, no dissipation is added to the modified system: the approximation of the conservative SGN system is also a conservative system. The advantage of such an approach is obvious: One can use for the dispersive SGN system the entire arsenal of numerical methods for hyperbolic equations. The method of "extended Lagrangian" was mathematically justified in Duchêne (2019). The method was succesfully used for other dispersive equations such as the nonlinear Schrödinger equation (Dhaouadi et al. 2019), the Benjamin–Bona–Mahony equation (Gavrilyuk and Shyue 2022), the Euler–van der Waals–Korteweg equations (Dhaouadi and Dumbser 2022), and thin film flows (Dhaouadi et al. 2022). Nonvariational hyperbolic approximation of the SGN equations also exist (Antuono et al. 2009; Mazaheri et al. 2016).

In this paper, we return to the idea of inverting the elliptic operator without the assumption of generalized potential flow: $\mathbf{K} \neq \nabla\phi$. The main result is that, even in 2D case, we have to invert only once the elliptic operator. The idea is based on the fact that, for the full Euler equations, one can obtain a scalar Poisson equation for pressure.

Combining this elliptic operator with the hyperbolic part of the equations yields a simple formulation of the algorithm, which can be implemented easily for accurate numerical resolution.

Derivation of the Averaged Pressure Equation

The 2D SGN [Eqs. (1a) and (1b)] are [with $\bar{\mathbf{v}} = (U, V)^T$ and $\mathbf{x} = (x, y)^T$]

$$h_t + (hU)_x + (hV)_y = 0 \tag{7a}$$

$$(hU)_t + \left(hU^2 + \frac{gh^2}{2} + h^2\left(\frac{1}{2}\ddot{b} + \frac{1}{3}\ddot{h}\right)\right)_x + (hUV)_y = -\left(gh + h\left(\ddot{b} + \frac{1}{2}\ddot{h}\right)\right) b_x \tag{7b}$$

$$(hV)_t + (hUV)_x + \left(hV^2 + \frac{gh^2}{2} + h^2\left(\frac{1}{2}\ddot{b} + \frac{1}{3}\ddot{h}\right)\right)_y = -\left(gh + h\left(\ddot{b} + \frac{1}{2}\ddot{h}\right)\right) b_y \tag{7c}$$

where U and V = the components in the x and y directions of the averaged over the fluid depth velocity. For convenience, we rewrite the momentum [Eqs. (7b) and (7c)] in the form

$$\begin{aligned} \dot{U} + \frac{1}{h}\left(\frac{gh^2}{2} + h^2\left(\frac{1}{2}\ddot{b} + \frac{1}{3}\ddot{h}\right)\right)_x &= -\left(g + \ddot{b} + \frac{1}{2}\ddot{h}\right) b_x \\ \dot{V} + \frac{1}{h}\left(\frac{gh^2}{2} + h^2\left(\frac{1}{2}\ddot{b} + \frac{1}{3}\ddot{h}\right)\right)_y &= -\left(g + \ddot{b} + \frac{1}{2}\ddot{h}\right) b_y \end{aligned} \tag{8}$$

Now, let P be the integrated fluid pressure divided by the constant density ρ and defined by

$$P = \frac{gh^2}{2} + h^2\left(\frac{1}{2}\ddot{b} + \frac{1}{3}\ddot{h}\right) \tag{9}$$

Then, we have

$$\begin{aligned} \dot{U} + \frac{P_x}{h} &= -\frac{1}{4}\left(g + \ddot{b} + \frac{6P}{h^2}\right) b_x \\ \dot{V} + \frac{P_y}{h} &= -\frac{1}{4}\left(g + \ddot{b} + \frac{6P}{h^2}\right) b_y \end{aligned} \tag{10}$$

Taking the divergence of the above system, we find

$$\nabla \cdot (\dot{\bar{\mathbf{v}}}) + \nabla \cdot \left(\frac{\nabla P}{h}\right) = \nabla \cdot \Psi \tag{11}$$

where

$$\bar{\mathbf{v}} = \begin{bmatrix} U \\ V \end{bmatrix}, \qquad \Psi = \begin{bmatrix} -(g + \ddot{b} + 6P/h^2) b_x/4 \\ -(g + \ddot{b} + 6P/h^2) b_y/4 \end{bmatrix} \tag{12}$$

The first term on the left-hand side of Eq. (11) becomes

$$\begin{aligned} \nabla \cdot (\dot{\bar{\mathbf{v}}}) &= \nabla \cdot \left(\frac{\partial \bar{\mathbf{v}}}{\partial t} + \frac{\partial \bar{\mathbf{v}}}{\partial \mathbf{x}} \bar{\mathbf{v}}\right) = \frac{\partial}{\partial t}(\nabla \cdot \bar{\mathbf{v}}) + \nabla \cdot \left(\frac{\partial \bar{\mathbf{v}}}{\partial \mathbf{x}} \bar{\mathbf{v}}\right) \\ &= \frac{\partial}{\partial t}(\nabla \cdot \bar{\mathbf{v}}) + \nabla \cdot \left(\frac{\partial \bar{\mathbf{v}}}{\partial \mathbf{x}}\right) \cdot \bar{\mathbf{v}} + \mathrm{trace}\left(\left(\frac{\partial \bar{\mathbf{v}}}{\partial \mathbf{x}}\right)^2\right) \\ &= \frac{\partial}{\partial t}(\nabla \cdot \bar{\mathbf{v}}) + \nabla(\nabla \cdot \bar{\mathbf{v}}) \cdot \bar{\mathbf{v}} + \mathrm{trace}\left(\left(\frac{\partial \bar{\mathbf{v}}}{\partial \mathbf{x}}\right)^2\right) \\ &= \overbrace{(\nabla \cdot \bar{\mathbf{v}})}^{\cdot} + \mathrm{trace}\left(\left(\frac{\partial \bar{\mathbf{v}}}{\partial \mathbf{x}}\right)^2\right) \\ &= \overbrace{(\nabla \cdot \bar{\mathbf{v}})}^{\cdot} + (\nabla \cdot \bar{\mathbf{v}})^2 - 2\det\left(\frac{\partial \bar{\mathbf{v}}}{\partial \mathbf{x}}\right) \end{aligned} \tag{13}$$

The last expression in the equation comes from

$$A^2 - \mathrm{trace}(A)A + \det(A)I = 0 \tag{14}$$

and

$$\mathrm{trace}(A^2) = (\mathrm{trace}(A))^2 - 2\det(A) \tag{15}$$

for a general 2×2 matrix A. Thus, we find an alternative form of Eq. (11)

$$\overbrace{(\nabla \cdot \bar{\mathbf{v}})}^{\cdot} + (\nabla \cdot \bar{\mathbf{v}})^2 - 2\det\left(\frac{\partial \bar{\mathbf{v}}}{\partial \mathbf{x}}\right) = -\nabla \cdot \left(\frac{\nabla P}{h}\right) + \nabla \cdot \Psi \tag{16}$$

Note that, from the mass conservation [Eq. (7*a*)], we have

$$\nabla \cdot \bar{\mathbf{v}} = -\frac{\dot{h}}{h} \tag{17}$$

Substituting Eq. (17) into Eq. (16), we find

$$\begin{aligned} -\nabla \cdot \left(\frac{\nabla P}{h}\right) + \nabla \cdot \Psi &= -\overbrace{\left(\frac{\dot{h}}{h}\right)}^{\cdot} + \left(\frac{\dot{h}}{h}\right)^2 - 2\det\left(\frac{\partial \bar{\mathbf{v}}}{\partial \mathbf{x}}\right) \\ &= -\frac{\ddot{h}}{h} + \frac{\dot{h}^2}{h^2} + \left(\frac{\dot{h}}{h}\right)^2 - 2\det\left(\frac{\partial \bar{\mathbf{v}}}{\partial \mathbf{x}}\right) \\ &= -\frac{\ddot{h}}{h} + 2\frac{\dot{h}^2}{h^2} - 2\det\left(\frac{\partial \bar{\mathbf{v}}}{\partial \mathbf{x}}\right) \end{aligned} \tag{18}$$

This leads to

$$\begin{aligned} \frac{1}{3}h^2\ddot{h} &= \frac{2}{3}h^3\left(\frac{\dot{h}^2}{h^2} - \det\left(\frac{\partial \bar{\mathbf{v}}}{\partial \mathbf{x}}\right)\right) + \frac{1}{3}h^3\nabla \cdot \left(\frac{\nabla P}{h}\right) - \frac{1}{3}h^3\nabla \cdot \Psi \\ &= P - \frac{1}{2}gh^2 - \frac{1}{2}h^2\ddot{b} \end{aligned} \tag{19}$$

We thus arrive at the scalar elliptic equation for the averaged pressure

$$\begin{aligned} &-\frac{h^3}{3}\nabla \cdot \left(\frac{\nabla P}{h}\right) - \frac{h^3}{2}\nabla \cdot \left(\frac{P\nabla b}{h^2}\right) + P \\ &\quad = \frac{2h^3}{3}\left[(\nabla \cdot \bar{\mathbf{v}})^2 - \det\left(\frac{\partial \bar{\mathbf{v}}}{\partial \mathbf{x}}\right)\right] + \frac{1}{2}gh^2 + \frac{1}{2}h^2\ddot{b} - \frac{h^3}{3}\nabla \cdot \Upsilon \end{aligned} \tag{20}$$

with

$$\Upsilon = \begin{bmatrix} -(g+\ddot{b})b_x/4 \\ -(g+\ddot{b})b_y/4 \end{bmatrix} \tag{21}$$

The elliptic operator for P can be rewritten in the form

$$-\frac{1}{3}\nabla \cdot \left(\frac{\nabla P}{h}\right) - \frac{1}{2}\left(\frac{\nabla P \cdot \nabla b}{h^2}\right) + P\left(\frac{1}{h^3} - \frac{1}{2}\mathrm{div}\left(\frac{\nabla b}{h^2}\right)\right) = f \tag{22}$$

where f = the right-hand side; and P verifies, for example, the Neumann or periodic condition at the boundary of the computational domain. The operator is invertible if $b(t, \mathbf{x})$ slowly varies and $h(t, \mathbf{x})$ is bounded from zero, i.e., the dry bottom case is avoided.

In the following, we consider the case of a stationary bottom topography $(b_t = 0)$. Then, we have

$$\begin{aligned} \dot{b} &= Ub_x + Vb_y, \\ \ddot{b} &= U(Ub_x + Vb_y)_x + V(Ub_x + Vb_y)_y \end{aligned} \tag{23}$$

For numerical purposes, it is more convenient to rewrite the governing equation in terms of a new variable ϖ, where $\varpi = P - gh^2/2$ is the averaged nonhydrostatic part of the physical pressure (divided by ρ). With ϖ, the 1D SGN model is

$$h_t + (hU)_x = 0 \tag{24a}$$

$$\begin{aligned} &(hU)_t + \left(hU^2 + \frac{1}{2}gh^2 + \varpi\right)_x \\ &\quad = -\left(gh + \frac{3}{2h}\varpi\right)b_x - \frac{1}{8}h[(Ub_x)^2]_x \end{aligned} \tag{24b}$$

$$\begin{aligned} &-\frac{h^3}{3}\left(\frac{\varpi_x}{h}\right)_x - \frac{h^3}{2}\left(\frac{b_x}{h^2}\varpi\right)_x + \varpi = \frac{2}{3}h^3U_x^2 \\ &\quad + \frac{1}{2}h^2U(Ub_x)_x + \frac{h^3}{3}\left[g(h+b)_x + \frac{1}{4}U(Ub_x)_x b_x\right]_x \end{aligned} \tag{24c}$$

In the 2D case, the governing equations written in terms of ϖ are

$$h_t + (hU)_x + (hV)_y = 0 \tag{25a}$$

$$\begin{aligned} &(hU)_t + \left(hU^2 + \frac{1}{2}gh^2 + \varpi\right)_x + (hUV)_y \\ &\quad = -\left(gh + \frac{3}{2h}\varpi\right)b_x - \frac{1}{4}h\ddot{b}b_x \end{aligned} \tag{25b}$$

$$\begin{aligned} &(hV)_t + (hUV)_x + \left(hV^2 + \frac{1}{2}gh^2 + \varpi\right)_y \\ &\quad = -\left(gh + \frac{3}{2h}\varpi\right)b_y - \frac{1}{4}h\ddot{b}b_y \end{aligned} \tag{25c}$$

$$\begin{aligned} &-\frac{h^3}{3}\left[\left(\frac{\varpi_x}{h}\right)_x + \left(\frac{\varpi_y}{h}\right)_y\right] - \frac{h^3}{2}\left[\left(\frac{b_x}{h^2}\varpi\right)_x + \left(\frac{b_y}{h^2}\varpi\right)_y\right] + \varpi \\ &= \frac{2h^3}{3}[(U_x + V_y)^2 - (U_xV_y - U_yV_x)] + \frac{h^2}{2}\ddot{b} \\ &\quad + \frac{h^3}{3}\left[\left(g(h+b)_x + \frac{1}{4}\ddot{b}b_x\right)_x + \left(g(h+b)_y + \frac{1}{4}\ddot{b}b_y\right)_y\right] \end{aligned} \tag{25d}$$

Numerical Method

To find approximate solutions to our SGN equations, we used a variant of the hyperbolic-elliptic splitting approach developed previously in Le Métayer et al. (2010) for $b = 0$. Our modified version of this algorithm will be presented in the form of two steps.

Hyperbolic step. At each intermediate stage of the semidiscrete scheme discussed as follows, we solve the hyperbolic part of the system written in compact vectorial form

$$\boldsymbol{q}_t + \mathrm{div}\mathcal{F}(\boldsymbol{q}) + \boldsymbol{\zeta}(\boldsymbol{q}, \nabla b) = \boldsymbol{\psi}(\boldsymbol{q}, \nabla \boldsymbol{q}, \nabla b, \nabla^2 b, \varpi, \nabla \varpi) \tag{26a}$$

where in two dimensions, for example, we have

$$\boldsymbol{q} = \begin{bmatrix} h \\ hU \\ hV \\ b \end{bmatrix}, \qquad \mathcal{F} = [\boldsymbol{F} \quad \boldsymbol{G}] = \begin{bmatrix} hU & hV \\ hU^2 + \frac{1}{2}gh^2 & hUV \\ hUV & hV^2 + \frac{1}{2}gh^2 \\ 0 & 0 \end{bmatrix} \tag{26b}$$

$$\boldsymbol{\zeta} = \begin{bmatrix} 0 \\ -ghb_x \\ -ghb_y \\ 0 \end{bmatrix}, \qquad \boldsymbol{\psi} = \begin{bmatrix} 0 \\ -\dfrac{3\varpi}{2h} b_x - \dfrac{h}{4}\ddot{b}b_x - \varpi_x \\ -\dfrac{3\varpi}{2h} b_y - \dfrac{h}{4}\ddot{b}b_y - \varpi_y \\ 0 \end{bmatrix} \tag{26c}$$

Elliptic step. Using the approximate solution $\boldsymbol{q}$ computed during the hyperbolic step, with the prescribed boundary conditions, we continue by inverting numerically the elliptic operator for ϖ written in the form

$$-\frac{h^3}{3}\nabla\cdot\left(\frac{1}{h}\nabla\varpi\right) - \frac{h^3}{2}\nabla\cdot\left(\frac{\nabla b}{h^2}\varpi\right) + \varpi = \varphi(\boldsymbol{q}, \nabla\boldsymbol{q}, \nabla^2\boldsymbol{q}, \nabla b, \nabla^2 b) \tag{27}$$

where φ is the right-hand side of Eqs. (24c) and (24d) for 1D and 2D problems, respectively.

Note that, in the hyperbolic step, rather than writing Eq. (26) with the fluxes $\boldsymbol{F}$ and $\boldsymbol{G}$ as a function of $\boldsymbol{q}$ and ϖ, we write it in the form with b included as an additional equation where the state-of-the-art well-balanced schemes for the Saint-Venant (SV) equations with the bottom topography can be used straightforwardly for the numerical resolution. We then obtain a standard elliptic problem, which any modern method can resolve (LeVeque 2007; Knabner and Angermann 2021; Steinbach 2007).

Hyperbolic Step

To numerically solve our SGN model in Eq. (26) in the hyperbolic step, we use the semidiscrete finite volume method written in a wave-propagation form (Ketcheson and LeVeque 2008; Ketcheson et al. 2013). We consider the 2D case as an exmple and describe the method on a uniform Cartesian grid of M cells with fixed mesh spacing Δx in the x direction and N cells with fixed mesh spacing Δy in the y direction. The method is based on a staggered grid formulation in which the value $\boldsymbol{Q}_{ij}(t)$ approximates the cell average of the solutions $\boldsymbol{q}$ over the grid cell C_{ij}

$$\boldsymbol{Q}_{ij}(t) \approx \frac{1}{\Delta x \Delta y}\int_{x_{i-\frac{1}{2}}}^{x_{i+\frac{1}{2}}}\int_{y_{j-\frac{1}{2}}}^{y_{j+\frac{1}{2}}} \boldsymbol{q}(t,x,y)dxdy \tag{28}$$

while $\Pi_{ij}(t) \approx \varpi(t, x_i, y_j)$ gives the pointwise approximation of the nonhydrostatic pressure ϖ at (x_i, y_j) at time t.

The semidiscrete version of the wave-propagation method is a method-of-lines discretization of Eq. (26) that can be written as a system of ordinary differential equations (ODEs) in the form

$$\frac{d\boldsymbol{Q}_{ij}}{dt} = \mathcal{L}_{ij}(\boldsymbol{Q}, \Pi) \tag{29a}$$

with

$$\mathcal{L}_{ij}(Q,\Pi) - \frac{1}{\Delta x}(\mathcal{A}^+\Delta Q_{i-\frac{1}{2},j} + \mathcal{A}^-\Delta Q_{i+\frac{1}{2},j} + \mathcal{A}\Delta Q_{ij}) - \frac{1}{\Delta y}(\mathcal{B}^+\Delta Q_{i,j-\frac{1}{2}} + \mathcal{B}^-\Delta Q_{i,j+\frac{1}{2}} + \mathcal{B}\Delta Q_{ij}) + \Psi_{ij}(\boldsymbol{Q},\Pi) \tag{29b}$$

for $i = 1, 2, \ldots, M$, $j = 1, 2, \ldots, N$. Here, $\boldsymbol{Q}$ and Π = the vectors with components $\boldsymbol{Q}_{ij}$ and Π_{ij}, respectively; $\mathcal{A}^+\Delta Q_{i-(1/2),j}$, $\mathcal{A}^-\Delta Q_{i+(1/2),j}$, $\mathcal{B}^+\Delta\boldsymbol{Q}_{i,j-(1/2)}$, and $\mathcal{B}^-\Delta\boldsymbol{Q}_{i,j+(1/2)}$ = the rightward-, leftward-, upward-, and downward-moving fluctuations; and $\mathcal{A}\Delta\boldsymbol{Q}_{ij}$ and $\mathcal{B}\Delta\boldsymbol{Q}_{ij}$ = the total fluctuations within the cell. To determine these fluctuations, we need to solve Riemann problems. Note that the term $\boldsymbol{\Psi}_{ij}(\boldsymbol{Q}, \Pi)$ in Eq. (29b) represents a discrete version of $\boldsymbol{\psi}$ over the grid cell C_{ij}, which can be evaluated straightforwardly by numerical differentiation techniques such as the finite-difference approximation of derivatives (LeVeque 2007).

Consider now the fluctuations $\mathcal{A}^{\pm}\Delta\boldsymbol{Q}_{i-(1/2),j}$ arising from the edge between cells $C_{i-1,j}$ and C_{ij}, for example. This amounts to solving the Cauchy problem for the homogeneous part of Eq. (26) in the x direction

$$\boldsymbol{q}_t + \boldsymbol{F}(\boldsymbol{q})_x + \boldsymbol{\zeta}(\boldsymbol{q}, b_x) = 0 \tag{30a}$$

with the piecewise constant initial data at a given time t_0

$$\boldsymbol{q}(t_0, x, y_j) = \begin{cases} \boldsymbol{q}^L_{i-\frac{1}{2},j} & \text{if } x < x_{i-\frac{1}{2}} \\ \boldsymbol{q}^R_{i-\frac{1}{2},j} & \text{if } x > x_{i-\frac{1}{2}} \end{cases} \tag{30b}$$

where $\boldsymbol{q}^L_{i-(1/2),j} = \lim_{x\to x_{(i-[1/2])^-}} \tilde{\boldsymbol{q}}_{i-1,j}(x)$ and $\boldsymbol{q}^R_{i-(1/2),j} = \lim_{x\to x_{(i-[1/2])^+}} \tilde{\boldsymbol{q}}_{i,j}(x)$ = the interpolated states obtained by taking limits of the reconstructed piecewise-continuous function $\tilde{\boldsymbol{q}}_{i-1,j}(x)$ or $\tilde{\boldsymbol{q}}_{i,j}(x)$ {each of them can be determined by applying a standard interpolation scheme to the set of discrete data $\{\boldsymbol{Q}_{ij}(t_0)\}$ [see Bouchut (2000), LeVeque (2002), and Shu (2009) for more details]} to the left and right of the cell edge at $x_{i-(1/2)}$, respectively.

Here, we are interested in the approximate Riemann solver of Roe (1981) for the numerical resolution of the Riemann problem. For that, we first write Eq. (26) as a quasilinear system of equations

$$\boldsymbol{q}_t + \mathcal{A}\boldsymbol{q}_x + \mathcal{B}\boldsymbol{q}_y = \boldsymbol{\psi}(\boldsymbol{q}, \nabla\boldsymbol{q}, \nabla b, \nabla^2 b, \varpi, \nabla\varpi) \tag{31a}$$

with

$$\mathcal{A} = \begin{bmatrix} 0 & 1 & 0 & 0 \\ -U^2 + gh & 2U & 0 & gh \\ -UV & V & U & 0 \\ 0 & 0 & 0 & 0 \end{bmatrix}, \quad \mathcal{B} = \begin{bmatrix} 0 & 0 & 1 & 0 \\ -UV & V & U & 0 \\ -V^2 + gh & 0 & 2V & gh \\ 0 & 0 & 0 & 0 \end{bmatrix} \tag{31b}$$

The eigenvalues and the corresponding eigenvectors of the matrices are, for matrix $\mathcal{A}$

$$\boldsymbol{\Lambda}_{\mathcal{A}} = \mathrm{diag}[\lambda_{\mathcal{A},1}, \lambda_{\mathcal{A},2}, \lambda_{\mathcal{A},3}, \lambda_{\mathcal{A},4}] = \mathrm{diag}[U - c, U, U + c, 0] \tag{32a}$$

$$\boldsymbol{R}_{\mathcal{A}} = [\boldsymbol{r}_{\mathcal{A},1}, \boldsymbol{r}_{\mathcal{A},2}, \boldsymbol{r}_{\mathcal{A},3}, \boldsymbol{r}_{\mathcal{A},4}] = \begin{bmatrix} 1 & 0 & 1 & c^2/(U^2 - c^2) \\ U - c & 0 & U + c & 0 \\ V & 1 & V & Vc^2/(U^2 - c^2) \\ 0 & 0 & 0 & 1 \end{bmatrix} \tag{32b}$$

and for matrix $\mathcal{B}$

$$\boldsymbol{\Lambda}_{\mathcal{B}} = \mathrm{diag}[\lambda_{\mathcal{B},1}, \lambda_{\mathcal{B},2}, \lambda_{\mathcal{B},3}, \lambda_{\mathcal{B},4}] = \mathrm{diag}[V - c, V, V + c, 0] \tag{32c}$$

J. Hydraul. Eng., 2024, 150(1): 04023054

$$\boldsymbol{R}_{\mathcal{B}} = [\boldsymbol{r}_{\mathcal{B},1}, \boldsymbol{r}_{\mathcal{B},2}, \boldsymbol{r}_{\mathcal{B},3}, \boldsymbol{r}_{\mathcal{B},4}] = \begin{bmatrix} 1 & 0 & 1 & c^2/(V^2-c^2) \\ U & 1 & U & Uc^2/(V^2-c^2) \\ V-c & 0 & V+c & 0 \\ 0 & 0 & 0 & 1 \end{bmatrix} \tag{32d}$$

where $c = \sqrt{gh}$, $\mathcal{A}\boldsymbol{R}_{\mathcal{A}} = \boldsymbol{\Lambda}_{\mathcal{A}}\boldsymbol{R}_{\mathcal{A}}$, and $\mathcal{B}\boldsymbol{R}_{\mathcal{B}} = \Lambda_{\mathcal{B}}R_{\mathcal{B}}$.

In a Roe's approximate Riemann solver, we replace the nonlinear system in Eq. (30a) with data $\boldsymbol{q}^L_{i-(1/2),j}$ and $\boldsymbol{q}^R_{i-(1/2),j}$ by a linear system of the form

$$\boldsymbol{q}_t + \widehat{A}\left(\boldsymbol{q}^L_{i-\frac{1}{2},j}, \boldsymbol{q}^R_{i-\frac{1}{2},j}\right)\boldsymbol{q}_x = 0 \tag{33}$$

where $\widehat{A}(\boldsymbol{q}^L_{i-(1/2),j}, \boldsymbol{q}^R_{i-(1/2),j})$ is a constant matrix that depends on the initial data and is a local linearization of the matrix A in Eq. (31) about an average state [see Bouchut (2000), LeVeque (2002), and Toro (1997) for more details].

The solution of the linear problem in Eq. (33) consists of three discontinuities propagating at constant speeds and a stationary discontinuity at the cell egde. The jump across each discontinuity is a multiple of the eigenvector of the matrix $\widehat{\mathcal{A}}$, and the propagating speed is the corresponding eigenvalue. We thus have the expression for the fluctuations as

$$\mathcal{A}^{\pm}\Delta Q_{i-\frac{1}{2},j} = \sum_{k1}^{4}\left(\widehat{\lambda}^{\mathcal{A},k}_{i-\frac{1}{2},j}\right)^{\pm}\widehat{\mathcal{W}}^{\mathcal{A},k}_{i-\frac{1}{2},j} \tag{34a}$$

where

$$\Delta\boldsymbol{q}_{i-\frac{1}{2},j} = \boldsymbol{q}^R_{i-\frac{1}{2},j} - \boldsymbol{q}^L_{i-\frac{1}{2},j} = \sum_{k=1}^{4}\widehat{\alpha}^{\mathcal{A},k}_{i-\frac{1}{2},j}\widehat{\boldsymbol{r}}^{\mathcal{A},k}_{i-\frac{1}{2},j} = \sum_{k=1}^{4}\widehat{\mathcal{W}}^{\mathcal{A},k}_{i-\frac{1}{2},j} \tag{34b}$$

with $\widehat{\mathcal{W}}^{\mathcal{A},k}_{i-(1/2),j}\widehat{\alpha}^k_{i-(1/2),j}\widehat{r}^k_{i-(1/2),j}$ for $k = 1, 2, 3, 4$, and

$$\widehat{\lambda}^{A,1}_{i-\frac{1}{2},j} = \widehat{U} - \widehat{c}, \qquad \widehat{\lambda}^{A,2}_{i-\frac{1}{2},j} = \widehat{U}, \qquad \widehat{\lambda}^{A,3}_{i-\frac{1}{2},j} = \widehat{U} + \widehat{c}, \qquad \widehat{\lambda}^{A,4}_{i-\frac{1}{2},j} = 0 \tag{34c}$$

$$\widehat{\alpha}^{A,1}_{i-\frac{1}{2},j} = \frac{1}{2\widehat{c}}\left[(\widehat{U}+\widehat{c})\Delta\boldsymbol{q}^{(1)}_{i-\frac{1}{2},j} - \Delta\boldsymbol{q}^{(2)}_{i-\frac{1}{2},j} - \left(\frac{\widehat{c}^2}{\widehat{U}-\widehat{c}}\right)\Delta\boldsymbol{q}^{(4)}_{i-\frac{1}{2},j}\right] \tag{34d}$$

$$\widehat{\alpha}^{A,2}_{i-\frac{1}{2},j} = -\widehat{V}\Delta\boldsymbol{q}^{(1)}_{i-\frac{1}{2},j} + \Delta\boldsymbol{q}^{(3)}_{i-\frac{1}{2},j} \tag{34e}$$

$$\widehat{\alpha}^{A,3}_{i-\frac{1}{2},j} = \frac{1}{2\widehat{c}}\left[-(\widehat{U}-\widehat{c})\Delta\boldsymbol{q}^{(1)}_{i-\frac{1}{2},j} + \Delta\boldsymbol{q}^{(2)}_{i-\frac{1}{2},j} + \left(\frac{\widehat{c}^2}{\widehat{U}+\widehat{c}}\right)\Delta\boldsymbol{q}^{(4)}_{i-\frac{1}{2},j}\right] \tag{34f}$$

$$\widehat{\alpha}^{A,4}_{i-\frac{1}{2},j} = \Delta\boldsymbol{q}^{(4)}_{i-\frac{1}{2},j} \tag{34g}$$

Here, we set $\widehat{U}$ and $\widehat{V}$ using the "Roe-averaging" approach based on data $q^L_{i-(1/2),j}$ and $q^R_{i-(1/2),j}$, and $\widehat{c}$ the arithmetic average of $c^L_{i-(1/2),j}$ and $c^R_{i-(1/2),j}$. The notation $\Delta\boldsymbol{q}^{(\iota)}_{i-(1/2),j}$ means the lth component of $\Delta\boldsymbol{q}_{i-(1/2),j}$. As usual, the quantities $s^{\pm}$ are set by $s^+ = \max(s, 0)$ and $s^- = \min(s, 0)$.

Similarly, by assuming that $b_x = 0$ at the center edge, we can define fluctuation $\mathcal{A}\Delta\boldsymbol{Q}_{ij}$ within cell C_{ij} based on the solution of the following Riemann problem:

$$\boldsymbol{q}_t + \boldsymbol{F}(\boldsymbol{q})_x = 0 \tag{35a}$$

with the initial condition

$$\boldsymbol{q}(t_0, x, y) = \begin{cases} \boldsymbol{q}^R_{i-\frac{1}{2},j} & \text{if } x < x_i \\ \boldsymbol{q}^L_{i+\frac{1}{2},j} & \text{if } x > x_i \end{cases} \tag{35b}$$

which gives $\Delta\boldsymbol{q}_{ij} = \boldsymbol{q}^L_{i+\frac{1}{2},j} - \boldsymbol{q}^R_{i-\frac{1}{2},j} = \sum_{k=1}^{4}\widehat{\alpha}^{\mathcal{A},k}_{ij}\widehat{r}^{\mathcal{A},k}_{ij} = \sum_{k=1}^{4}\widehat{\mathcal{W}}^{\mathcal{A},k}_{ij}$, yielding

$$\mathcal{A}\Delta Q_{ij} = \sum_{k=1}^{4}(\widehat{\lambda}^{\mathcal{A},k}_{ij})^{\pm}\widehat{\mathcal{W}}^{\mathcal{A},k}_{ij} \tag{35c}$$

Analogously, we can find the remaining fluctuations $\mathcal{B}^{\pm}\Delta\boldsymbol{Q}_{i,j+(1/2)}$ and $\mathcal{B}\Delta\boldsymbol{Q}_{ij}$ by solving the homogeneous part of Eq. (26) in the y direction with the piecewise constant data at the cell edge.

To integrate the system of ODEs in Eq. (29a) in time, we employ the strong stability-preserving (SSP) multistage Runge–Kutta scheme (Gottlieb et al. 2001). That is, in the first-order case we use the Euler forward time discretization as

$$\boldsymbol{Q}^{n+1}_{ij} = \boldsymbol{Q}^n_{ij} + \Delta t\mathcal{L}_{ij}(\boldsymbol{Q}^n, \Pi^n) \tag{36a}$$

where we start with the cell average $\boldsymbol{Q}^n_{ij} \approx \boldsymbol{Q}_{ij}(t_n)$ and $\Pi^n_{ij} \approx \varpi(t_n, x_i, y_j)$ at time t_n, yielding the solution at the next time step $\boldsymbol{Q}^{n+1}_{ij}$ over $\Delta t = t_{n+1} - t_n$. In the second-order case, however, we use the classical two-stage Heun method (also called the modified Euler method) as

$$\begin{aligned} \boldsymbol{Q}^*_{ij} &= \boldsymbol{Q}^n_{ij} + \Delta t\mathcal{L}_{ij}(\boldsymbol{Q}^n, \Pi^n), \\ \boldsymbol{Q}^{n+1}_{ij} &= \frac{1}{2}\boldsymbol{Q}^n_{ij} + \frac{1}{2}\boldsymbol{Q}^*_{ij} + \frac{1}{2}\Delta t\mathcal{L}_{ij}(\boldsymbol{Q}^*, \Pi^*) \end{aligned} \tag{36b}$$

It is common that the three-stage third-order scheme of the form

$$\begin{aligned} \boldsymbol{Q}^*_{ij} &= \boldsymbol{Q}^n_{ij} + \Delta t\mathcal{L}_{ij}(\boldsymbol{Q}^n, \Pi^n) \\ \boldsymbol{Q}^{**}_{ij} &= \frac{3}{4}\boldsymbol{Q}^n_{ij} + \frac{1}{4}\boldsymbol{Q}^*_{ij} + \frac{1}{4}\Delta t\mathcal{L}_{ij}(\boldsymbol{Q}^*, \Pi^*) \\ \boldsymbol{Q}^{n+1}_{ij} &= \frac{1}{3}\boldsymbol{Q}^n_{ij} + \frac{2}{3}\boldsymbol{Q}^*_{ij} + \frac{2}{3}\Delta t\mathcal{L}_{ij}(\boldsymbol{Q}^{**}, \Pi^{**}) \end{aligned} \tag{36c}$$

is a preferred one to be used in conjunction with the third- or fifth-order weighted essentially nonoscillatory (WENO) scheme (Shu 2009). It is important to note that we update Π after each intermediate ODE stage.

Elliptic Step

To discuss discretizations, we consider the elliptic Eq. (27) in two dimensions and problems subject to the prescribed boundary conditions. Asssume that $\boldsymbol{q}$ is known a priori from the hyperbolic step at a given time. We will describe a five-point finite difference method on a uniform Cartesian grid with mesh spacing Δx and Δy as before (LeVeque 2007; Knabner and Angermann 2021). To discretize Eq. (27), for terms on the left-hand side, we replace the second-order derivative by taking a backward difference for the outer derivative and then a forward difference for the inner derivative and the first-order derivative by taking a centered difference; for terms on the left-hand side, we use centered difference for all the derivatives. Collecting terms, we obtain the following constant coefficient difference formula for node ij:

$$\alpha_{ij}\Pi_{i-1,j}+\beta_{ij}\Pi_{i+1,j}+\gamma_{ij}\Pi_{i,j-1}+\delta_{ij}\Pi_{i,j+1}+\eta_{ij}\Pi_{ij}=\Phi_{ij} \tag{37}$$

with α_{ij}, β_{ij}, γ_{ij}, δ_{ij}, η_{ij}, and φ_{ij} defined by

$$\alpha_{ij}=-\frac{H_{ij}^3}{3(\Delta x)^2}\left(\frac{1}{H_{i-\frac{1}{2},j}}-\frac{3}{4H_{i-1,j}^2}(b_{i,j}-b_{i-1,j})\right)$$

$$\beta_{ij}=-\frac{H_{ij}^3}{3(\Delta x)^2}\left(\frac{1}{H_{i+\frac{1}{2},j}}+\frac{3}{4H_{i+1,j}^2}(b_{i+1,j}-b_{i,j})\right)$$

$$\gamma_{ij}=-\frac{H_{ij}^3}{3(\Delta y)^2}\left(\frac{1}{H_{i,j-\frac{1}{2}}}-\frac{3}{4H_{i,j-1}^2}(b_{i,j}-b_{i,j-1})\right)$$

$$\delta_{ij}=-\frac{H_{ij}^3}{3(\Delta y)^2}\left(\frac{1}{H_{i,j+\frac{1}{2}}}+\frac{3}{4H_{i,j+1}^2}(b_{i,j+1}-b_{i,j})\right)$$

$$\eta_{ij}=\frac{H_{ij}^3}{3(\Delta x)^2}\left(\frac{1}{H_{i-\frac{1}{2},j}}+\frac{1}{H_{i+\frac{1}{2},j}}\right)+\frac{H_{ij}^3}{3(\Delta y)^2}\left(\frac{1}{H_{i,j-\frac{1}{2}}}+\frac{1}{H_{i,i+\frac{1}{2},j}}\right)+1$$

$$\begin{aligned}\Phi_{ij}=&\frac{2H_{ij}^3}{3}((\mathcal{D}\cdot\mathcal{U}_{ij})^2-\det(\mathcal{D}U_{ij},\mathcal{D}V_{ij}))\\&+\frac{H_{ij}^2}{2}(\mathcal{U}_{ij}\cdot\mathcal{D}(\mathcal{U}_{ij}\cdot\mathcal{D}b_{ij}))+\frac{gH_{ij}^3}{3}\mathcal{D}\cdot\mathcal{D}(H+b)_{ij}\\&+\frac{H_{ij}^3}{12}\mathcal{D}\cdot\mathcal{D}((\mathcal{U}_{ij}\cdot\mathcal{D}(\mathcal{U}_{ij}\cdot\mathcal{D}b_{ij}))b_{ij})\end{aligned} \tag{38}$$

respectively. Here, $\mathcal{U}_{ij}=(U_{ij},V_{ij})$ = the numerical approximation of the velocity vector (U,V) at (x_i,y_j); and $\mathcal{D}=(\boldsymbol{D}_{x,0},\boldsymbol{D}_{y,0})$ = the discrete gradient operator with $\boldsymbol{D}_{x,0}$ and $\boldsymbol{D}_{y,0}$ the second-order centered difference for the first derivatives in the x and y directions, respectively (LeVeque 2007). The notations $H_{i\pm(1/2),j}$, $H_{i,j\pm(1/2)}$, $b_{i\pm1,j}$, and $b_{i,j\pm1}$ are the pointwise approximate values at the respective spatial locations.

Going through all the nodal points for $i=1,2,\ldots,M$, and $j=1,2,\ldots,N$, incorporating the boundary conditions, we have a linear system of $M\times N$ unknowns $\Pi(t)$, which would be a strictly diagonal dominant linear system if $b(t,\mathbf{x})$ slowly varies, which can be solved by the state-of-the-art iterative methods (Trefethen and Bau 1997).

Well-Balanced Condition

Assume that the lake is at rest, where $U=V=0$ at all times. From Eq. (25), we find a simplified steady-state system

$$\left(\frac{1}{2}gh^2+\varpi\right)_x=-\left(gh+\frac{3}{2h}\varpi\right)b_x \tag{39a}$$

$$\left(\frac{1}{2}gh^2+\varpi\right)_y=-\left(gh+\frac{3}{2h}\varpi\right)b_y \tag{39b}$$

$$\begin{aligned}-\frac{h^3}{3}\left[\left(\frac{\varpi_x}{h}\right)_x+\left(\frac{\varpi_y}{h}\right)_y\right]-\frac{h^3}{2}\left[\left(\frac{b_x}{h^2}\varpi\right)_x+\left(\frac{b_y}{h^2}\varpi\right)_y\right]\\+\varpi=\frac{gh^3}{3}\nabla^2(h+b)\end{aligned} \tag{39c}$$

Now, we write the [Eqs. (39a) and (39b)] in the form

$$\begin{aligned}gh(h+b)_x&=-\frac{3}{2h}\varpi b_x-\varpi_x\\gh(h+b)_y&=-\frac{3}{2h}\varpi b_y-\varpi_y\end{aligned} \tag{40}$$

and find easily the equilibrium free surface $h+b$ = constant at all times if $\varpi=0$ is the solution of the elliptic [Eq. (39c)]. Inversly, to preserve $h+b$ = constant, we must have

$$\varpi_x=-\frac{3}{2h}\varpi b_x \quad\text{and}\quad \varpi_y=-\frac{3}{2h}\varpi b_y \tag{41}$$

Substituting the equations into Eq. (39c), we have

$$\varpi=\frac{gh^3}{3}\nabla^2(h+b)=0 \tag{42}$$

The fact the $\varpi=0$ is equivalent to $b+h$ = const means the SGN model reduces to the SV equations for the lake-at-rest problem (Michel-Dansac et al. 2016).

Numerical Examples

We begin by considering two benchmark tests with the flat bottom where the exact solution or the "true" solution obtained from a simplified model is readily avaliable for comparison. In all the tests, the gravitational constant was chosen to be $g=9.81\ \mathrm{m/s^2}$, and the Courant number was set to 0.5 to ensure stability of the hyperbolic solver.

Propagation of a Solitary Wave

Our first test is the numerical accuracy study for the propagation of a single solitary wave over a flat bottom in one dimension. The exact solution of the problem with respect to $\xi=x-Dt$ is: for the height

$$h(\xi)=h_1+(h_2-h_1)\mathrm{sech}^2\left(\frac{(\xi-x_0)}{2}\sqrt{\frac{3(h_2-h_1)}{h_2h_1^2}}\right) \tag{43a}$$

for the velocity

Table 1. Numerical results for the solitary wave problem obtained using our algorithm with four different mesh sizes and four different hyperbolic integration schemes; one-norm errors in the height and the two-norm errors in the nonhydrostatic pressure ϖ are shown at time $t=100/D$ s. The elliptic equation in Eq. (24c) is solved using second-order finite difference scheme in all cases

Godunov	$E^1(h)$	Order	$E^2(\varpi)$	Order
$N=1{,}000$	4.930×10^{-1}	—	1.707×10^{-1}	—
$N=2{,}000$	3.103×10^{-1}	0.67	1.132×10^{-1}	0.59
$N=4{,}000$	1.783×10^{-1}	0.80	6.722×10^{-2}	0.75
$N=8{,}000$	9.632×10^{-2}	0.89	3.700×10^{-2}	0.86
MUSCL				
$N=1{,}000$	2.679×10^{-2}	—	9.209×10^{-3}	—
$N=2{,}000$	6.928×10^{-3}	1.95	2.327×10^{-3}	1.98
$N=4{,}000$	1.793×10^{-3}	1.95	6.709×10^{-4}	1.79
$N=8{,}000$	5.490×10^{-4}	1.71	3.492×10^{-4}	0.94
WENO 3				
$N=1{,}000$	7.664×10^{-3}	—	4.992×10^{-3}	—
$N=2{,}000$	1.431×10^{-3}	2.42	9.121×10^{-4}	2.45
$N=4{,}000$	2.844×10^{-4}	2.33	1.736×10^{-4}	2.39
$N=8{,}000$	6.214×10^{-5}	2.19	3.624×10^{-5}	2.26
BVD 35				
$N=1{,}000$	3.446×10^{-3}	—	1.491×10^{-3}	—
$N=2{,}000$	8.642×10^{-4}	2.00	3.730×10^{-4}	2.00
$N=4{,}000$	2.163×10^{-4}	2.00	9.329×10^{-5}	2.00
$N=8{,}000$	5.409×10^{-5}	2.00	2.333×10^{-5}	2.00

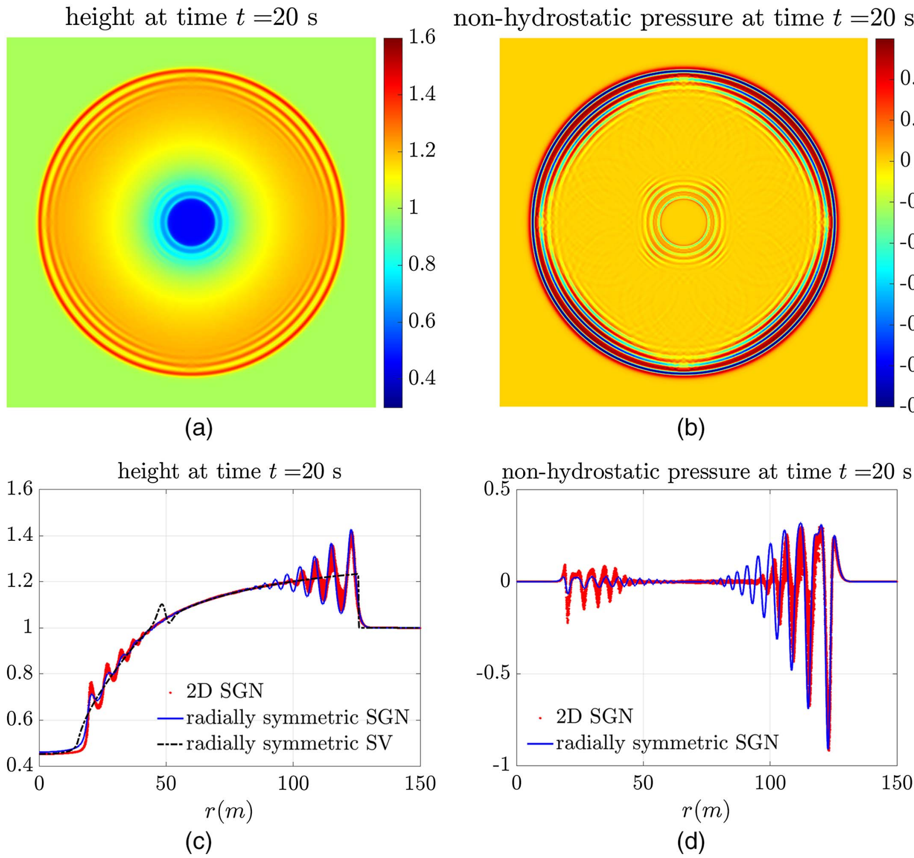

Fig. 2. Results for a radially symmetric problem at time $t = 20$ s. Top figures: images of the height and the nonhydrostatic pressure ϖ. Bottom figures: scatter plots of the height and ϖ. The solid line in the scatter plot is the "true" solution obtained from solving the radially symmetric SGN model with appropriate source terms for the radial symmetry; the dashed line is the results obtained using the SV equation, where $\varpi = 0$. The dotted points are the 2D result.

$$U(\xi) = D\left(1 - \frac{h_1}{h(\xi)}\right) \tag{43b}$$

and for the nonhydrostatic pressure ϖ

$$\varpi(\xi) = \frac{1}{3} g h_1^2 h_2 h(\xi) \left(\frac{h'(\xi)}{h(\xi)}\right)' \tag{43c}$$

where h_1 and h_2 = the fluid depth at infinity and under the soliton's crest; x_0 = the initial location of the soliton; and $D = \sqrt{gh_2}$ = the wave speed. We set $x_0 = 0$, $h_1 = 1$ m, and $h_2 = 1.2$ m, yielding D ≈ 3.431 m/s; the computational domain is of size 100 m with periodic boundary conditions at both ends.

Table 1 shows one-norm errors of the height at time $t = 100/D \approx 29.1457$ s (time necessary to the crest of the solitary wave to travel one period) for a convergence study of the solutions obtained using our numerical strategy with four different mesh sizes $N = 1{,}000$, 2,000, 4,000, and 8,000, and four different hyperbolic integration schemes. The underlying elliptic solver for Eq. (27) is the second-order finite difference scheme, which can be inverted straightforwardily.

Let $E^p(w) = \{E_j^p(w)\}$ for $j = 1, 2, 3, 4$ be the sequence of the p-norm error of the computed solution w to its true solution on an $N = \{1{,}000, 2{,}000, 4{,}000, 8{,}000\}$ grid. With that, it is a common practice (LeVeque 2007) to estimate the rate of convergence for w using the errors on

$$\text{convergence order} = \frac{\ln(E_{j-1}^p(w)/E_j^p(w))}{\ln(N_{j-1}/N_j)} \tag{44}$$

From Table 1, for the one-norm errors for height and two-norm errors for the nonhydrostatic pressure ϖ, we observe that, when the Godunov method is employed in the hyperbolic step (i.e., the method uses zeroth-order piecewise constant

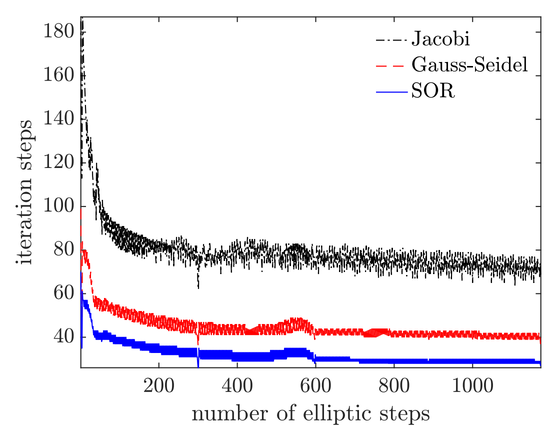

Fig. 3. Convergence study of the Jacobi, Gauss–Seidel, and SOR methods for inverting the elliptic operator to the 2D radial-symmetric solution shown in Fig. 2. Here, the number of iteration steps in total during each elliptic-step run is shown.

reconstruction scheme for the Riemann data at the cell edges, and the forward Euler method in Eq. (36*a*) for the time discretization), the order of accuracy of algorithm approaches to first-order accurate as the mesh is refined. When monotonic upstream-centered scheme for conservation laws (MUSCL) is employed alternatively [i.e., the first-order piecewise linear reconstruction scheme with the monotinized centered limiter and the Heun method in Eq. (36*b*) are in use], the convergence rate is not second-order accurate as the mesh is refined. In the WENO 3 case, however [i.e., the method uses the third-order WENO scheme for Riemann data reconstruction, and the third-order method in Eq. (36*c*) for the time discretization], the order of accuracy is slightly greater than 2 in h and ϖ, which is less than 3 (the formal order of accuracy of the hyperbolic solver WENO 3); this result may not come as a surprise because our underlying elliptic solver is only of $O((\Delta x)^2)$. In the boundary variation diminishing (BVD) 35 case, where the method employs the third-order SSP scheme in the time integration together with the pair of third- and fifth-order WENO scheme in the BVD reconstruction process (Deng et al. 2018), we found the same convergence behavior as in the WENO 3 case. Nevertheless, among all three methods, BVD 35 gives the smallest error in magnitude for each mesh size.

Thus, in all the test cases, the computation was carried out using our algorithm with the BVD 35 scheme in the hyperbolic part and the second-order finite difference method in the elliptic part.

Note that, in Gavrilyuk et al. (2020), we have conducted a similar numerical accuracy study of the solitary wave propagation using the K-based SGN equations, also observing sensible convergence behavior as we refine the mesh.

Radially Symmetric Problem

Our second example is a radially symmetric problem; this problem was studied in Tkachenko et al. (2023) as an example for the

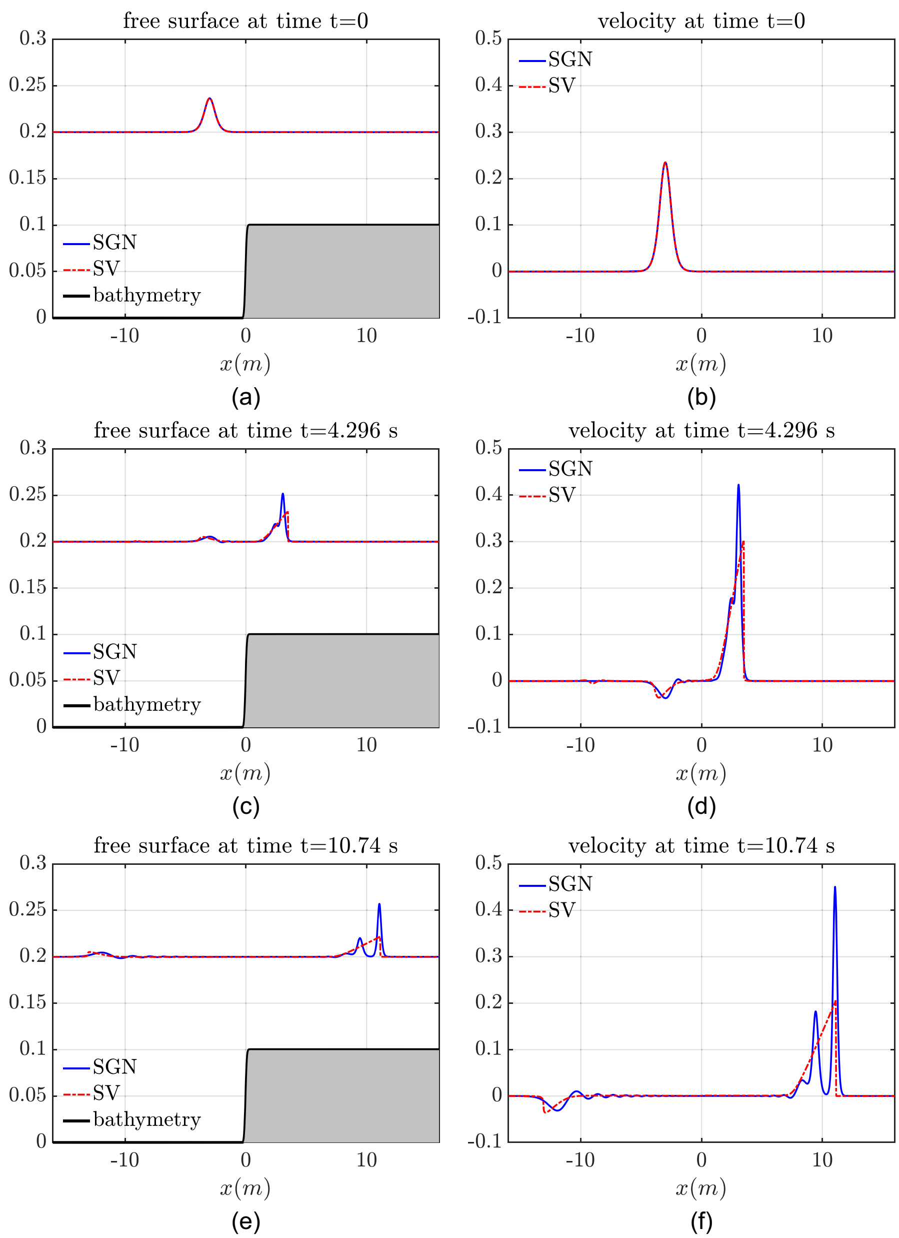

Fig. 4. Results for a solitary wave over a step. Numerical solutions of the free surface $h + b$ and the velocity u for both the SGN and SV models are shown at three different times $t = 0$, 4.296 s, and 10.74 s.

numerical validation of a hyperbolized SGN model. Initially, the fluid is at rest in the entire computational domain of size $(x,y)\epsilon[-150,150]\times[-150,150]$ m^2, $u(0,x,y)=0$ m/s, while its depth is a smooth function

$$h(0,r)=h_R+\frac{h_L-h_R}{2}\left(1+\tanh\left(\frac{r_0-r}{\alpha}\right)\right) \tag{45}$$

where we take $\alpha=2$, where h_L, h_R, and $\alpha=1.8$ m, 1 m, and 2, respectively; $r=\sqrt{x^2+y^2}$; and $r_0=50$ m. Fig. 2 shows the pseudocolor images (top row) and the scatter plots (bottom row) of the height and the nonhydrostatic pressure ϖ at time $t=20$ s obtained using our algorithm with a 600×600 grid. From the plots, it is easy to observe that breaking of the cylindrical water column results in an outgoing circular dispersive shock wave and an incoming rarefaction wave. We observe also the good qualitative agreement of the results as compared with the "true" solution obtained from solving the 1D SGN model with appropriate source terms for the radial symmetry (Le Métayer et al. 2010) with 3,000 mesh points. For comparison, we also show the radially symmetric solution in the water height obtained using the SV equation ($\varpi=0$), observing the effect of the nonhydrostatic pressure to the solution.

To study the convergence of our iterative solver for the inversion of the 2D discrete elliptic operator (the 1D elliptic operator is inverted by a direct method), for simplicity, we consider the Jacobi, Gauss–Seidel, and the successive over-relaxation (SOR) methods, and employ each of them in the computations for comparison. In Fig. 3, we plot the number of iteration steps in total that were taken during each of elliptic steps until the stopping criteria is achieved for the convergence. Here, the stopping criteria we used is

$$\min_k(E_k^2(\mathbf{\Pi}),E_k^{\max}(\mathbf{\Pi}))\leq 10^{-d} \tag{46}$$

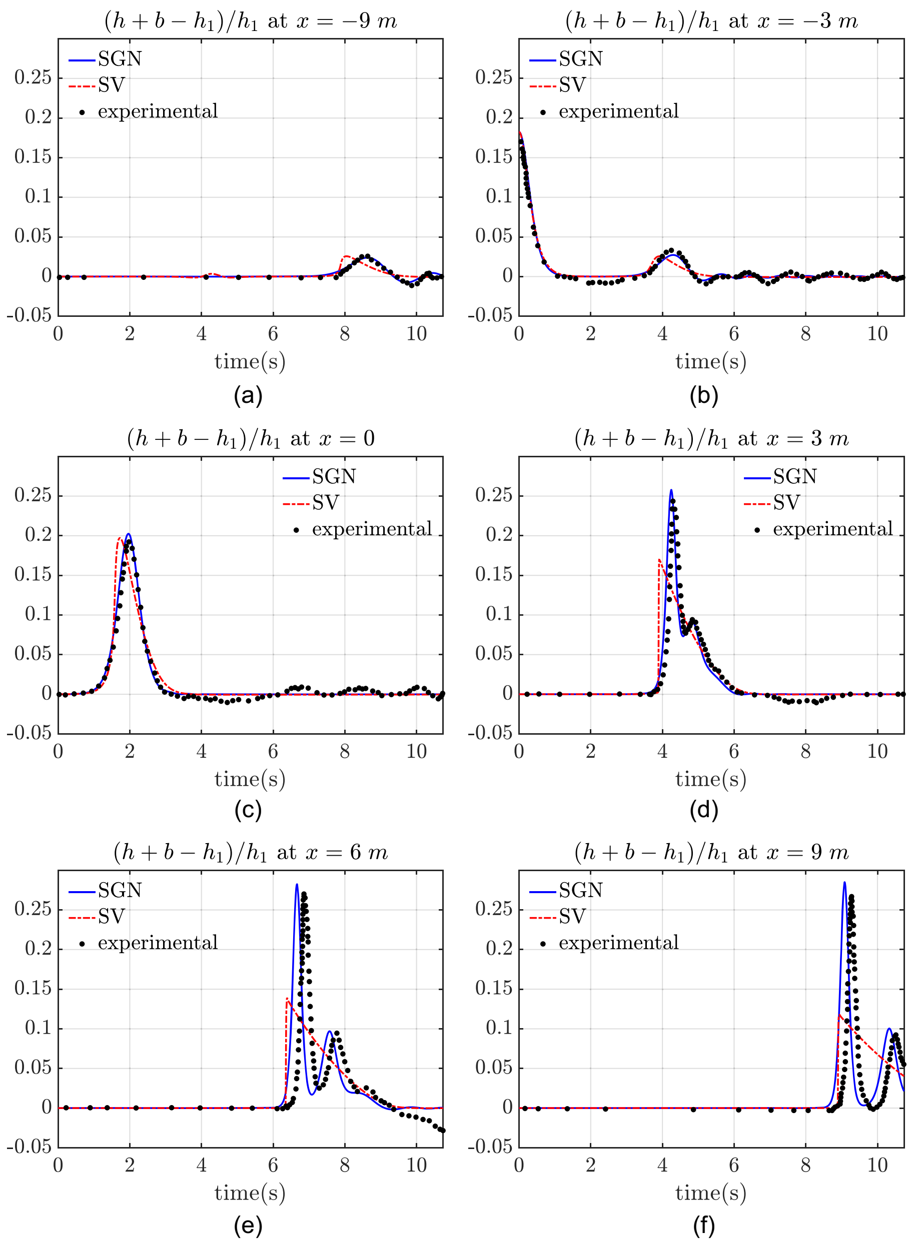

Fig. 5. Comparision of the time history of the wave-amplitude ratio $(h+b-h_1)/h_1$ and the experimental data at the gauge locations $x=-9$ m, -3 m, 0 m, 3 m, 6 m, and 9 m. Results for the SGN and SV models are shown.

where $E_k^2(\mathbf{\Pi}) = \|\mathbf{\Pi}_k - \mathbf{\Pi}_{k-1}\|_2$ and $E_k^{\max}(\mathbf{\Pi}) = \|\mathbf{\Pi}_k - \mathbf{\Pi}_{k-1}\|_{\max}$ = the two- and maximum-norm errors of Π at the kth iteration step, respectively; and $d = 6$. It is clear that our elliptic solver works satisfactorily with the SOR method and has faster convergence than the Jacobi and the Gauss–Seidel methods, which is expected (LeVeque 2007; Trefethen and Bau 1997). Here, a fixed relaxation facor $\omega = 1.2$ was chosen for the SOR method in the computations.

Solitary Wave over a Step

We continue by considering a benchmark test for the solitary wave over a step (Seabra-Santos et al. 1987), where the numerical results can be compared with the experimental data for the numerical validation. Here, for the solitary wave in Eq. (43), we use $x_0 = -3$ m, $h_1 = 0.2$ m, and $h_2 = 0.2365$ m; for the bathymetry, we take

$$b(x) = \frac{1}{20}(1 + \mathrm{erf}(8x)) \tag{47}$$

where erf is the error function (Abramowitz and Stegun 1964). The computational domain is $x \epsilon [-16, 16]$ m.

Fig. 4 shows the free surface $h + b$ and the velocity u at three different times $t = 0$, 4.296 s, and 10.74 s. We observe the smooth propagation of the soliton over the bathymetry, and the variation of the soliton profile as time proceeds. In addition, there is spurious oscillation observed in the solutions near the step; this gives an example showing that the lake-at-rest conditions are handled satisfactorily by our algorithm. The comparision of the time history of the wave-amplitude ratio $(h + b - h_1)/h_1$ and the experimental data at the gauge locations $x = -9$ m, -3 m, 0 m, 3 m, 6 m, and 9 m are shown in Fig. 5, observing good agreement of the results. The computation was carried out using our algorithm with 6,400 meshes, and nonreflecting outflow boundary condition was used on the left and right boundaries. In Figs. 4 and 5, numerical results obtained using the SV equation where $\varpi = 0$ are also included for comparison.

Solitary Wave over a Gaussian Hump

We are next concerned with the propagation of a solitary wave over a 2D Gaussian hump; this problem was studied in Busto et al. (2021) as an example for the numerical validation of a hyperbolized SGN model. Here, for the solitary wave in Eq. (43), we take $x_0 = -5$ m, $h_1 = 0.2$ m, and $h_2 = 0.2365$ m; for the bathymetry, we have

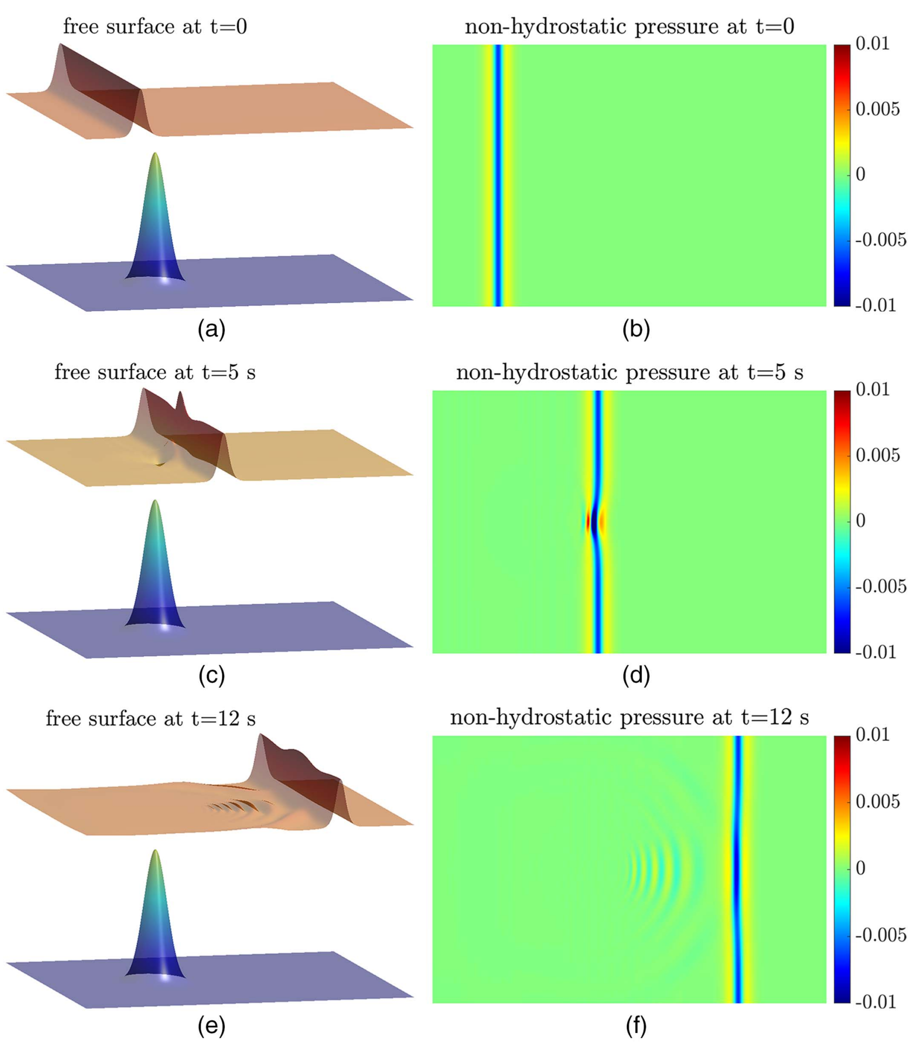

Fig. 6. Results for a solitary wave over a Gaussian hump at three different times $t = 0$, 5 s, and 12 s. Left figures: surface plots of the free surface $h + b$ together with the bathymetry are shown. In each graph, the free surface is on the top, and the bathymetry is on the bottom. Right figures: pseudocolor plots of the nonhydrostatic pressure ϖ.

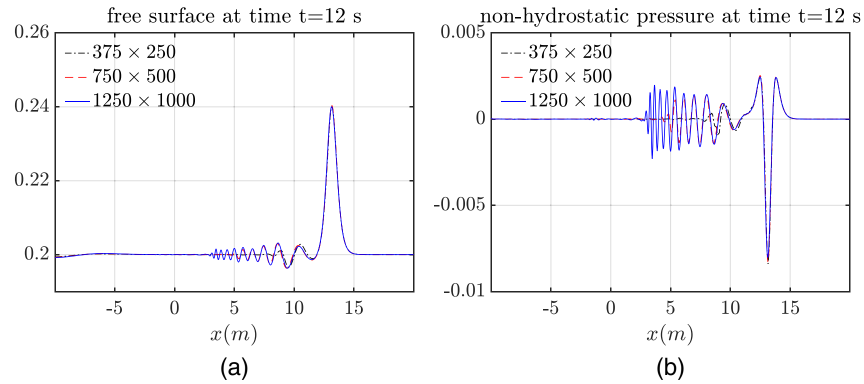

Fig. 7. Convergence study of the free surface and nonhydrostatic pressure ϖ for the solitary wave over a Gaussian hump. The test is performed using three different grid systems: 375×250, 750×500, and $1{,}250 \times 1{,}000$; the solutions are plotted along $y = 0$ at time $t = 20$ s.

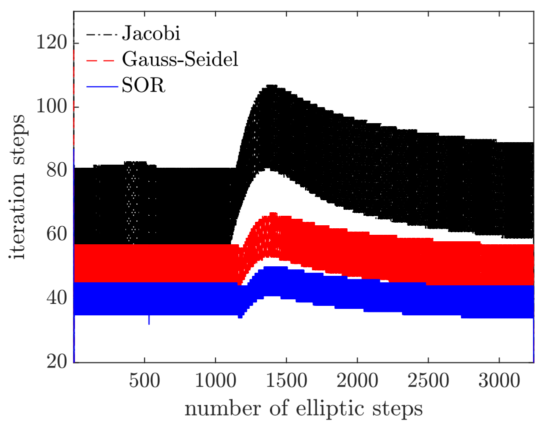

Fig. 8. Convergence study of the Jacobi, Gauss–Seidel, and the SOR methods for inverting the elliptic operator to the solution shown in Fig. 6. Here, the number of iteration steps in total during each elliptic-step run are shown.

$$b(x,y) = \frac{1}{10}\exp\left(-\frac{x^2+y^2}{2}\right) \tag{48}$$

The computational domain is $(x,y)\epsilon[-10,20]\times[-10,10]$ m^2. Fig. 6 shows numerical results of the free surface $h+b$ (left figures) and the nonhydrostatic pressure ϖ (right figures) at times $t=0$, 5 s, and 12 s obtained using our algorithm with 750×500 mesh points. We observe the growth of the soliton amplitude as it propagated over the hump, and the formation of transmitted and reflected waves afterward. We also observe the smooth solution transition across the bottom topography, which gives another example showing that our algorithm is a well-balanced scheme. In Fig. 7, we show results for a convergence study of $h+b$ and ϖ at time 12 s along $y=0$ using three different meshes: 375×250, 750×500, and $1{,}250\times 1{,}000$, observing qualitatively agreement of the solutions as the mesh is refined. To study the convergence of our iterative solver for the inversion of the 2D discrete elliptic operator with the bottom topography, Fig. 8 shows the number of iteration steps in total for the Jacobi, Gauss–Seidel, and the SOR methods in each elliptic-step run. The faster convergence of the SOR method, as compared with the Jacobi and the Gauss–Seidel method, is again observed.

Conclusion

The SGN equation is the best representative of the so-called Boussinesq–type models describing dispersive shallow water flows. They predict much better specific features of wave propagation and interaction compared with the classical hydrostatic SV equations. We have proposed a simple hyperbolic-elliptic splitting approach for the numerical resolution of the SGN equations in 1D and 2D problems with the bottom topography. The algorithm uses a state-of-the-art well-balanced scheme for the hyperbolic part of the equations, and a stationary iterative method such as the Jacobi, Gauss–Seidel, and SOR methods for the inversion of the elliptic operator for the nonhydrostatic part of the pressure, yielding an efficient implementation of the algorithm. Sample numerical results presented in the paper show the feasibility of the algorithm to practical problems. Ongoing works aim at extending this approach to breaking waves and to the cases with more general boundary conditions.

Appendix. Derivation of the SGN Equations

We denote the time with t and the Cartesian coordinate axes by x_k for $k \in \{1, 2, \ldots, d\}$ with d being the space dimension. Sometimes, we will also make use of the notation $x \coloneqq x_1$, $y \coloneqq x_2$, and $z \coloneqq x_3$.

We present a rapid derivation of the SGN equations by Hamilton's principle. Consider the Euler equations of incompressible fluids between the rigid bottom $z = b(t, x_1, x_2)$ and free surface $z = h(t, x_1, x_2) + b(t, x_1, x_2)$ (Fig. 1)

$$\mathrm{div}_2\mathbf{v} + \frac{\partial v_3}{\partial z} = 0, \qquad \rho\frac{D\mathbf{v}}{Dt} + \nabla_2 p = 0, \qquad \rho\frac{Dv_3}{Dt} + \frac{\partial p}{\partial z} = -\rho g \tag{49}$$

where $(\mathbf{v}, v_3)^T$ = the velocity field; $\mathbf{v} = (v_1, v_2)^T$ = the horizontal velocity; v_3 = the vertical component of the velocity; g = the gravity acceleration; the divergence and gradient operators are taken with respect to x_1, x_2 variables (this is denoted with Index 2); ρ = the fluid density; p = the pressure; and $(D/Dt) = (\partial/\partial t) + \mathbf{v}\cdot\nabla_2 + v_3(\partial/\partial z)$ = the material derivative. The standard boundary conditions are fulfilled at the free surface:

$$(h+b)_t + \mathbf{v}\cdot\nabla_2(h+b) = v_3, \quad p = 0 \tag{50}$$

and at the bottom

$$b_t + \mathbf{v} \cdot \nabla_2 b = v_3 \tag{51}$$

Consider the following dimensionless variables (with "tilde"):

$$(x_1, x_2) \to L(\tilde{x}_1, \tilde{x}_2), \qquad x_3 \to L\tilde{x}_3, \qquad t \to \frac{L}{\sqrt{gH}}\tilde{t},$$
$$\mathbf{v} \to \sqrt{gH}\tilde{\mathbf{v}}, \qquad v_3 \to \varepsilon\sqrt{gH}\tilde{v}_3, \qquad p \to \rho g H \tilde{p}, \qquad b \to H\tilde{b} \tag{52}$$

Here, the small parameter $\varepsilon = H/L$ = the ratio of the vertical scale height H and horizontal scale length L (Fig. 1). In shallow water, approximation of the dimensionless equations become (we will suppress the "tilde" for the dimensionless variables)

$$\mathrm{div}_2\mathbf{v} + \frac{\partial v_3}{\partial z} = 0, \qquad \frac{D\mathbf{v}}{Dt} + \nabla_2 p = 0, \qquad \varepsilon^2\frac{Dv_3}{Dt} + \frac{\partial p}{\partial z} = -1 \tag{53}$$

The boundary conditions have the same form in dimensionless variables.

The corresponding total energy of the flow can be written as

$$\mathcal{E} = \int_{-\infty}^{+\infty}\int_{-\infty}^{+\infty}\int_{b}^{b+h}\left(\frac{|\mathbf{v}|^2 + \varepsilon^2 v_3^2}{2} + z + C\right)dz dx_1 dx_2 \tag{54}$$

where constant C is added to have a finite total energy in the class of solutions having the same constant values at infinity ($\mathbf{v} \to \mathbf{0}$, $h \to h_\infty$, $b \to 0$). The incompressibility equation and kinematic boundary conditions imply the mass conservation law in the form

$$h_t + \mathrm{div}(h\bar{\mathbf{v}}) = 0, \qquad h\bar{\mathbf{v}} = \int_b^{b+h}\mathbf{v}dz \tag{55}$$

In the following, "dot" = the material derivative along the averaged velocity $\bar{\mathbf{v}}$: for any function $f(t, x_1, x_2)$, we denote

$$\dot{f} = \left(\frac{\partial}{\partial t} + \bar{\mathbf{v}} \cdot \nabla\right)f, \qquad \ddot{f} = \left(\frac{\partial}{\partial t} + \bar{\mathbf{v}} \cdot \nabla\right)^2 f \tag{56}$$

Since the averaged quantities depend only on t, x_1, x_2, we will no longer use the index "two" with the space operators. To derive the equations, we do not need the assumption of potential flow. It can be replaced by a weaker condition: the horizontal vorticity is of order ε^s, with $s > 1$ [see Barros et al. (2007) for details]. The velocity v_3 can be presented by the following approximate expression:

$$v_3 \approx \dot{b} - (z - b)\mathrm{div}(\bar{\mathbf{v}}) = \dot{b} + \frac{z - b}{h}\dot{h} \tag{57}$$

Then, up to ε^2 order terms, one has (Barros et al. 2007)

$$\int_b^{b+h}\left(\frac{|\mathbf{v}|^2 + \varepsilon^2 v_3^2}{2} + z\right)dz \approx h\left(\frac{|\bar{\mathbf{v}}|^2}{2} + \frac{\varepsilon^2}{6}\left(\dot{h} + \frac{3}{2}\dot{b}\right)^2 + \frac{\varepsilon^2}{8}\dot{b}^2\right) + \frac{h}{2}(2b + h) \tag{58}$$

It allows us to write the Lagrangian (difference between kinetic and potential energy) in the form

$$\mathcal{L} = \int_{-\infty}^{+\infty}\int_{-\infty}^{+\infty} L dx_1 dx_2 \tag{59}$$

with

$$L(\bar{\mathbf{v}}, h, \dot{h}, b, \dot{b}) = h\left(\frac{|\bar{\mathbf{v}}|^2}{2} + \frac{\varepsilon^2}{6}\left(\dot{h} + \frac{3}{2}\dot{b}\right)^2 + \frac{\varepsilon^2}{8}\dot{b}^2\right) - \frac{h}{2}(h + 2b) - Ch \tag{60}$$

The corresponding Hamilton's action between the time instants t_0 and t_1 is then

$$a = \int_{t_0}^{t_1}\mathcal{L}dt \tag{61}$$

The Euler–Lagrange equations for Eq. (61) under the constraint in Eq. (55) can be obtained by the method developed in Barros et al. (2007), Gavrilyuk (2011), and Dhaouadi et al. (2019). One can obtain the following momentum equation of the second order of accuracy with respect to ε:

$$(h\bar{\mathbf{v}})_t + \mathrm{div}\left(h\bar{\mathbf{v}} \otimes \bar{\mathbf{v}} + \left(\frac{h^2}{2} + \varepsilon^2 h^2\left(\frac{1}{2}\ddot{b} + \frac{1}{3}\ddot{h}\right)\right)\mathbf{I}\right) = -p|_{z=b}\nabla b \tag{62}$$

with

$$p|_{z=b} = h + \varepsilon^2 h\left(\ddot{b} + \frac{1}{2}\ddot{h}\right) \tag{63}$$

Eqs. (55), (62), and (63) admit the energy conservation law

$$(h\mathcal{E})_t + \mathrm{div}\left(h\bar{\mathbf{v}}\mathcal{E} + \left(\frac{h^2}{2} + \varepsilon^2 h^2\left(\frac{1}{2}\ddot{b} + \frac{1}{3}\ddot{h}\right)\right)\bar{\mathbf{v}}\right) = p|_{z=b}b_t \tag{64}$$

where

$$\mathcal{E} = \frac{|\bar{\mathbf{v}}|^2}{2} + \frac{h}{2} + b + \varepsilon^2\left(\frac{1}{6}\left(\dot{h} + \frac{3}{2}\dot{b}\right)^2 + \frac{1}{8}\dot{b}^2\right) \tag{65}$$

Thus, in the case of a stationary bottom topography [$b = b(\mathbf{x})$], the energy conservation law is exact. The mathematical justification of the SGN equations is given in Makarenko (1986) and Lannes (2013). For completeness, we will now write the SGN equations in dimensional form

$$h_t + \mathrm{div}(h\bar{\mathbf{v}}) = 0 \tag{66a}$$

$$(h\bar{\mathbf{v}})_t + \mathrm{div}\left(h\bar{\mathbf{v}} \otimes \bar{\mathbf{v}} + \left(\frac{gh^2}{2} + \frac{h^2}{3}\left(\ddot{h} + \frac{3}{2}\ddot{b}\right)\right)\mathbf{I}\right) = -p|_{z=b}\nabla b \tag{66b}$$

$$(h\mathcal{E})_t + \mathrm{div}\left(h\bar{\mathbf{v}}\mathcal{E} + \left(\frac{gh^2}{2} + \frac{h^2}{3}\left(\ddot{h} + \frac{3}{2}\ddot{b}\right)\right)\bar{\mathbf{v}}\right) = p|_{z=b}b_t \tag{66c}$$

with

$$p|_{z=b} = gh + h\left(\ddot{b} + \frac{1}{2}\ddot{h}\right) \tag{66d}$$

$$\mathcal{E} = \frac{|\bar{\mathbf{v}}|^2}{2} + g\left(\frac{h}{2} + b\right) + \frac{1}{6}\left(\dot{h} + \frac{3}{2}\dot{b}\right)^2 + \frac{1}{8}\dot{b}^2 \tag{66e}$$

where $p|_{z=b}$ is the physical bottom pressure divided by ρ.

Data Availability Statement

The computational codes developed for this research are available from the authors by request.

Acknowledgments

The authors would like to thank the reviewers of this paper for their important comments and suggestions. KMS was partially supported by the Grant MOST 110-2115-M-002-004-MY2.

References

Abramowitz, M., and I. A. Stegun. 1964. *Handbook of mathematical functions with formulas, graphs, and mathematical tables*. New York: Dover.

Antuono, M., V. Liapidevskii, and M. Brocchini. 2009. "Dispersive nonlinear shallow-water equations." *Stud. Appl. Math.* 122 (1): 1–28. https://doi.org/10.1111/j.1467-9590.2008.00422.x.

Barros, R., S. Gavrilyuk, and V. Teshukov. 2007. "Dispersive nonlinear waves in two-layer flows with free surface. I: Model derivation and general properties." *Stud. Appl. Math.* 119 (3): 191–211. https://doi.org/10.1111/j.1467-9590.2007.00383.x.

Bazdenkov, S., N. Morozov, and O. Pogutse. 1987. "Dispersive effects in two-dimensional hydrodynamics." *Sov. Phys. Dokl.* 32 (Apr): 262.

Bouchut, F. 2000. *Nonlinear stability of finite volume methods for hyperbolic conservation laws and well-balanced schemes for sources*. Basel, Switzerland: Birkhauser.

Busto, S., M. Dumbser, C. Escalante, N. Favrie, and S. Gavrilyuk. 2021. "On high order ADER discontinuous Galerkin schemes for first order hyperbolic reformulations of nonlinear dispersive systems." *J. Sci. Comput.* 87 (2): 48. https://doi.org/10.1007/s10915-021-01429-8.

Camassa, R., D. D. Holm, and C. D. Levermore. 1996. "Long-time effects of bottom topography in shallow water." *Phys. D* 98 (2–4): 258–286. https://doi.org/10.1016/0167-2789(96)00117-0.

Cantero-Chinchilla, F. N., O. Castro-Orgaz, S. Dey, and J. L. Ayuso-Munoz. 2016. "Nonhydrostatic dam break flows. I: Physical equations and numerical schemes." *J. Hydraul. Eng.* 142 (12): 4016068. https://doi.org/10.1061/(ASCE)HY.1943-7900.0001205.

Castro-Orgaz, O., and W. H. Hager. 2017. *Non-hydrostatic free surface flows*. Berlin: Springer.

Castro-Orgaz, O., W. H. Hager, and F. N. Cantero-Chinchilla. 2022. "Shallow flows over curved beds: Application of the Serre-Green-Naghdi theory to weir flow." *J. Hydraul. Eng.* 148 (1): 4021053. https://doi.org/10.1061/(ASCE)HY.1943-7900.000195.

Castro-Orgaz, O., W. H. Hager, and N. D. Katapodes. 2023. "Variational models for nonhydrostatic free-surface flow: A unified outlook to maritime and open-channel hydraulics developments." *J. Hydraul. Eng.* 149 (7): 04023014. https://doi.org/10.1061/JHEND8.HYENG-13338.

Cienfuegos, R. 2023. "Surfing waves from the ocean to the river with the serre-green6naghdi equations." *J. Hydraul. Eng.* 149 (9): 04023032. https://doi.org/10.1061/JHEND8.HYENG-13487.

Deng, X., S. Inaba, B. Xie, K.-M. Shyue, and F. Xiao. 2018. "High fidelity discontinuity-resolving reconstruction for compressible multiphase flows with moving interfaces." *J. Comput. Phys.* 371 (Oct): 945–966. https://doi.org/10.1016/j.jcp.2018.03.036.

Dhaouadi, F., and M. Dumbser. 2022. "A first order hyperbolic reformulation of the Navier-Stokes-Korteweg system based on the GPR model and an augmented Lagrangian approach." *J. Comp. Phys.* 470 (Dec): 111544. https://doi.org/10.1016/j.jcp.2022.111544.

Dhaouadi, F., N. Favrie, and S. Gavrilyuk. 2019. "Extended Lagrangian approach for the defocusing nonlinear Schrödinger equation." *Stud. Appl. Math.* 142 (3): 336–358. https://doi.org/10.1111/sapm.12238.

Dhaouadi, F., S. Gavrilyuk, and J.-P. Vila. 2022. "Hyperbolic relaxation models for thin films down an inclined plane." *Appl. Math. Comput.* 433 (Nov): 127378. https://doi.org/10.1016/j.amc.2022.127378.

Duchêne, V. 2019. "Rigorous justification of the Favrie-Gavrilyuk approximation to the Serre-Green-Naghdi model." *Nonlinearity* 32 (10): 3772–3797. https://doi.org/10.1088/1361-6544/ab22fb.

Favrie, N., and S. Gavrilyuk. 2017. "A rapid numerical method for solving Serre-Green-Naghdi equations describing long free surface gravity waves." *Nonlinearity* 30 (7): 2718. https://doi.org/10.1088/1361-6544/aa712d.

Gavrilyuk, S. 2011. "Multiphase flow modelling via Hamilton's principle." In *Variational models and methods in solid and fluid mechanics*, edited by F. dell'Isola and S. Gavrilyuk. Berlin: Springer.

Gavrilyuk, S., H. Kalisch, and Z. Khorsand. 2014. "A kinematic conservation law in free surface flow." *Nonlinearity* 28 (6): 1805–1821. https://doi.org/10.1088/0951-7715/28/6/1805.

Gavrilyuk, S., B. Nkonga, K.-M. Shyue, and L. Truskinovsky. 2020. "Stationary shock-like transition fronts in dispersive systems." *Nonlinearity* 33 (10): 5477–5509. https://doi.org/10.1088/1361-6544/ab95ac.

Gavrilyuk, S., and K.-M. Shyue. 2022. "Hyperbolic approximation of the BBM equation." *Nonlinearity* 35 (3): 1447. https://doi.org/10.1088/1361-6544/ac4c49.

Gavrilyuk, S., and V. M. Teshukov. 2001. "Generalized vorticity for bubbly liquid and dispersive shallow water equations." *Continuum Mech. Thermodyn.* 13 (6): 365–382. https://doi.org/10.1007/s001610100057.

Gottlieb, S., C. W. Shu, and E. Tadmor. 2001. "Strong stability preserving high-order time discretization methods." *SIAM Rev.* 43 (1): 89–112. https://doi.org/10.1137/S003614450036757X.

Green, A. E., N. Laws, and P. M. Naghdi. 1974. "On the theory of water waves." *Proc. R. Soc. London, Ser. A* 338 (1612): 43–55. https://doi.org/10.1098/rspa.1974.0072.

Green, A. E., and P. M. Naghdi. 1976. "A derivation of equations for wave propagation in water of variable depth." *J. Fluid Mech.* 78 (2): 237–246. https://doi.org/10.1017/S0022112076002425.

Ketcheson, D. I., and R. J. LeVeque. 2008. "WENOCLAW: A higher order wave propagation method." In *Hyperbolic problems: Theory, numerics, applications*, 609–616. Berlin: Springer.

Ketcheson, D. I., M. Parsani, and R. J. LeVeque. 2013. "High-order wave propagation algorithm for hyperbolic systems." *SIAM J. Sci. Comput.* 35 (1): 351–377. https://doi.org/10.1137/110830320.

Knabner, P., and L. Angermann. 2021. *Numerical methods for elliptic and parabolic partial differential equations*. Berlin: Springer.

Lannes, D. 2013. *The water waves problem*. Amer, India. Mathematical Surveys and Monographs.

Le Métayer, O., S. Gavrilyuk, and S. Hank. 2010. "A numerical scheme for the Green-Naghdi model." *J. Comp. Phys.* 229 (6): 2034–2045. https://doi.org/10.1016/j.jcp.2009.11.021.

LeVeque, R. J. 2002. *Finite volume methods for hyperbolic problems*. Cambridge, MA: Cambridge University Press.

LeVeque, R. J. 2007. *Finite difference methods for ordinary and partial differential equations: Steady-state and time-dependent problems*. Philadelphia, PA: Society for Industrial and Applied Mathematics.

Li, M., P. Guyenne, F. Li, and L. Xu. 2014. "High order well-balanced CDG-FE methods for shallow water waves by a Green-Naghdi model." *J. Comput. Phys.* 257 (Jan): 169–192. https://doi.org/10.1016/j.jcp.2013.09.050.

Li, M., L. Xu, and Y. Cheng. 2019. "A CDG-FE method for the two-dimensional Green-Naghdi model with the enhanced dispersive property." *J. Comput. Phys.* 399 (Dec): 108953. https://doi.org/10.1016/j.jcp.2019.108953.

Liapidevskii, V. Y., and K. N. Gavrilova. 2008. "Dispersion and blockage effects in the flow over a sill." *J. Appl. Mech. Tech. Phys.* 49 (Jan): 34–45. https://doi.org/10.1007/s10808-008-0005-7.

Makarenko, N. 1986. "A second long-wave approximation in the Cauchy-Poisson problem." [In Russian.] *Dyn. Contin. Media* 77 (91): 56–72.

Marche, F. 2020. "Combined hybridizable discontinuous Galerkin (HDG) and Runge-Kutta discontinuous Galerkin (RK-DG) formulations for Green-Naghdi equations on unstructured meshes." *J. Comp. Phys.* 418 (Oct): 109637. https://doi.org/10.1016/j.jcp.2020.109637.

Mazaheri, A., M. Ricchiuto, and H. Nishikawa. 2016. "A first-order hyperbolic system approach for dispersion." *J. Comput. Phys.* 321 (Sep): 593–605. https://doi.org/10.1016/j.jcp.2016.06.001.

Michel-Dansac, V., C. Berthon, S. Clain, and F. Foucher. 2016. “A well-balanced scheme for the shallow-water equations with topography.” *Comput. Math. Appl.* 72 (3): 568–593. https://doi.org/10.1016/j.camwa.2016.05.015.

Miles, J., and R. Salmon. 1985. “Weakly dispersive nonlinear gravity waves.” *J. Fluid Mech.* 157 (Aug): 519–531. https://doi.org/10.1017/S0022112085002488.

Roe, P. L. 1981. “Approximate Riemann solvers, parameter vector, and difference scheme.” *J. Comput. Phys.* 43 (2): 357–372. https://doi.org/10.1016/0021-9991(81)90128-5.

Salmon, R. 1998. *Lectures on geophysical fluid dynamics*. Oxford, UK: Oxford University Press.

Seabra-Santos, F. J., D. P. Renouard, and A. M. Temperville. 1987. “Numerical and experimental study of the transformation of a solitary wave over a shelf or isolated obstacle.” *J. Fluid Mech.* 176 (Mar): 117–134. https://doi.org/10.1017/S0022112087000594.

Serre, F. 1953. “Contribution à l’étude des écoulements permanents et variables dans les canaux.” *Houille Blanche* 39 (Dec): 374–388. https://doi.org/10.1051/lhb/1953034.

Shu, C. W. 2009. “High order weighted essentially nonoscillatory schemes for convection dominated problems.” *SIAM Rev.* 51 (1): 82–126. https://doi.org/10.1137/070679065.

Steinbach, O. 2007. *Numerical approximation methods for elliptic boundary value problems: Finite and boundary elements*. Berlin: Springer.

Su, C. H., and C. S. Gardner. 1969. “Korteweg-de Vries equation and generalisations. III: Derivation of the Korteweg—De Vries equation and Burgers equation.” *J. Math. Phys.* 10 (3): 536–539. https://doi.org/10.1063/1.1664873.

Tkachenko, S., S. Gavrilyuk, and J. Massoni. 2023. “Extended Lagrangian approach for the numerical study of multidimensional dispersive waves: Applications to the Serre-Green-Naghdi equations.” *J. Comput. Phys.* 477 (Mar): 111901. https://doi.org/10.1016/j.jcp.2022.111901.

Toro, E. F. 1997. *Riemann solvers and numerical methods for fluid dynamics*. Berlin: Springer.

Trefethen, L. N., and I. D. Bau. 1997. *Numerical linear algebra*. Philadelphia, PA: Society for Industrial and Applied Mathematics.